

Visually-Guided Controllable Medical Image Generation via Fine-Grained Semantic Disentanglement

Xin Huang^{1,2,†}, Junjie Liang^{1,2,†}, Qingshan Hou^{1,2}, Peng Cao^{1,2,3(✉)}, Jinzhu Yang^{1,2,3}, Xiaoli Liu⁴, and Osmar R. Zaiane⁵

¹ Computer Science and Engineering, Northeastern University, Shenyang, China

² Key Laboratory of Intelligent Computing in Medical Image of Ministry of Education, Northeastern University, Shenyang, China

³ National Frontiers Science Center for Industrial Intelligence and Systems Optimization, Shenyang, China
caopeng@cse.neu.edu.cn

⁴ AiShiWeiLai AI Research, China

⁵ Amii, University of Alberta, Edmonton, Alberta, Canada

Abstract. Medical image synthesis is crucial for alleviating data scarcity and privacy constraints. However, fine-tuning general text-to-image (T2I) models remains challenging, mainly due to the significant modality gap between complex visual details and abstract clinical text. In addition, semantic entanglement persists, where coarse-grained text embeddings blur the boundary between anatomical structures and imaging styles, thus weakening controllability during generation. To address this, we propose a Visually-Guided Text Disentanglement framework. We introduce a cross-modal latent alignment mechanism that leverages visual priors to explicitly disentangle unstructured text into independent semantic representations. Subsequently, a Hybrid Feature Fusion Module (HFFM) injects these features into a Diffusion Transformer (DiT) through separated channels, enabling fine-grained structural control. Experimental results in three datasets demonstrate that our method outperforms existing approaches in terms of generation quality and significantly improves performance on downstream classification tasks. The source code is available at <https://github.com/hx111/VG-MedGen>.

Keywords: Medical Image Synthesis · Diffusion Transformer · Cross-Modal Alignment · Data Augmentation

1 Introduction

High-quality annotated medical imaging datasets form the foundation for developing robust artificial intelligence (AI)-assisted diagnostic systems. However, acquiring such data remains challenging due to the scarcity of rare medical cases, the high cost of expert annotations, and strict privacy regulations[19,11,6]. To

[†] The two authors contribute equally to this work.

Input Prompt	Med-Art	Ours	Comparative Analysis	Model Complexity & Efficiency
<p>A dermoscopic image of a nevus showing a dark brownish-red, highly irregular and asymmetrical lesion with a sharp, well-defined border. The texture presents a dense pigment network with heterogeneous structure.</p>			<p>Med-Art: Fails morphological control: generates a symmetrical, uniform, and smooth-edged blob.</p> <p>Ours: Precise highly irregular asymmetry, sharp well-defined borders, accurate heterogeneous internal structure.</p>	<p>Params: 5.457M (Transformer 611M + T5 4.762M + VAE 84M) Inference: 2.574 ± 0.005 sec/image Memory: ~10.9 GB (FP16)</p>
<p>A dermoscopic image of Vascular_Lesion: A distinct red circular lesion with a slightly raised border, exhibiting a speckled texture. The surrounding skin has a pinkish hue and is slightly raised, with fine white lines extending outward from the edge of the lesion, giving a sense of asymmetry.</p>			<p>Med-Art: Blurred lesion boundaries, oversmoothed appearance, weak contrast, and missing fine vascular texture.</p> <p>Ours: Clear lesion boundary, realistic color distribution, preserved vascular details, and natural dermoscopic texture.</p>	
<p>A dermoscopic image of Benign_Keratosis features a brown to dark brown, irregularly shaped lesion with a wavy border. The texture appears granular and the background is a pinkish-brown color. The lesion has a symmetrical shape with a central area of darker brown. The dermoscopic patterns include a central, circular, brown to dark brown area with a lighter halo. The background shows pinkish-brown speckles and a fine, wispy texture.</p>			<p>Med-Art: Simple dark spot, uniform color, lacks structural composition.</p> <p>Ours: Distinct central darker area, clear lighter halo, faithful wispy background texture and pinkish-brown speckles.</p>	

Fig. 1. Impact of text prompts for comparable methods on image synthesis. Anatomical structures and modality styles are highlighted in red and blue, respectively.

mitigate these challenges, Generative AI, particularly Latent Diffusion Models (LDM) [17] and their Transformer-based variants, such as DiT [14], have gradually emerged as an effective approach to data enhancement. By conditioning themselves on textual descriptions, these models are able to synthesize diverse medical images, offering new opportunities to alleviate long-tailed medical distributions [13,8,21].

Despite recent progress in adapting general-purpose text-to-image models to the medical domain [4,10], existing approaches still exhibit limited anatomical controllability. This limitation primarily stems from the intrinsic semantic granularity gap between medical images and clinical text: images encode rich spatial and geometric details, while text is highly compressed, providing insufficient guidance for fine-grained structure generation. Moreover, commonly used text encoders produce global semantic embeddings in which structural and textural styles are implicitly averaged, blurring their boundaries in the latent space. As illustrated in Fig. 1, despite explicit prompts regardless of prompt lengths, details specific structural (e.g., irregular shape) and textural styles, models such as Med-Art fail to generate images with these characteristics. The generated images disregard both the desired irregularity and internal texture, indicating that structural cues are progressively diluted during diffusion. Such anatomically implausible generations substantially limit the effectiveness of synthetic data for improving downstream diagnostic robustness. Moreover, these models are computationally expensive, whereas our method reduces inference parameters to 833M (84.7% fewer compared with Med-Art) and achieves 1.457s per image (1.77× faster), enabling efficient clinical deployment.

To address these issues, we propose a Visually-Guided Text Disentanglement Diffusion Framework. Our core insight is that, although textual representations are inherently abstract and susceptible to entanglement, the visual features are

- We design a cross-modal latent alignment strategy and a hybrid feature fusion module, enabling the generative model to learn fine-grained, biologically plausible features directly from unstructured text. Our model is designed to be lightweight, requiring fewer parameters during inference.
- Extensive experiments on three medical datasets demonstrate that our method outperforms existing approaches in generation quality and diversity. Notably, the synthesized data yields significant performance gains in downstream classification tasks.

2 Method

2.1 Visual Attribute Captioning

To mitigate the semantic sparsity of existing medical datasets, which lack fine-grained visual descriptions, we construct an automated attribute captioning pipeline using LLaVA-Next [12]. We design constrained prompt templates to suppress hallucinations, explicitly directing the VLM to focus on two orthogonal dimensions: Anatomy (e.g., symmetry, boundary, shape) and Style (e.g., color distribution, texture patterns). The prompt follows a structured format: "Describe the [Class] image using features: [Attribute List]". Subsequently, a T5 model [16] refines the generated descriptions. This process yields high-quality image-text pairs rich in structural and textural style details, providing robust priors for the subsequent cross-modal alignment.

2.2 Visually-Guided Text Disentanglement & Alignment

To resolve the high semantic entanglement between anatomical structures and modality styles in medical text, we design a visually-guided cross-modal disentanglement module. This module leverages the inherent fine-grained visual features as supervisory to guide the text encoder to map unstructured text into disentangled semantic representations in the latent space.

Visual Disentanglement. We construct a dual-branch visual encoder to extract anatomical and style representations from medical images. As illustrated in Fig.2, given an input image x , the Image Anatomy Encoder E_a^I [18] adopts a U-Net-based architecture to capture spatial and geometric structures such as lesion shape and boundaries. Its output feature map \hat{f}_a^I is constrained by a lightweight segmentation head with a Dice loss \mathcal{L}_{dice} . This explicit supervision encourages E_a^I to focus exclusively on anatomical structure. Meanwhile, the Image Style Encoder E_s^I models imaging appearance attributes including texture, color, and intensity. Following a variational formulation, E_s^I is implemented as a convolutional encoder that takes the concatenation of the input image x and the extracted anatomical feature \hat{f}_a^I as input, and maps it into a Gaussian latent distribution parameterized by (μ, σ) . A latent style code \hat{f}_s^I is then sampled via the reparameterization trick. The Kullback–Leibler divergence loss \mathcal{L}_{kl} is applied to regularize the style latent space toward a standard normal distribution,

ensuring smoothness and continuity. To maintain information integrity, an image decoder D^I is introduced to reconstruct the original image from the disentangled representations. The overall objective function for the visual disentanglement is defined as:

$$\mathcal{L}_{img} = \mathcal{L}_{rec}^I + \lambda_{dice}\mathcal{L}_{dice} + \lambda_{kl}\mathcal{L}_{kl} \quad (1)$$

Text Disentanglement & Cross-Modal Alignment. After training the visual branch, all visual encoders are frozen to serve as stable and reliable supervision signals. Given a textual description generated by a vision-language model (VLM), we first extract a base semantic embedding using a frozen ClinicalBERT encoder [2]. To endow the text representation with disentanglement capability, we design two text mapping networks: a text anatomy encoder E_a^T and a text style encoder E_s^T . Unlike convolutional visual encoders, both E_a^T and E_s^T are implemented as lightweight multi-layer perceptrons, each consisting of two fully connected layers with ReLU activation and dropout. These networks operate as projection heads that map the global, entangled semantic embedding into low-dimensional latent spaces corresponding to anatomical structure and imaging style, respectively. The core of this module lies in the cross-modal latent alignment mechanism. Specifically, we enforce the text anatomical representation f_a^T to align with the visual anatomical feature f_a^I , while the text style representation f_s^T is aligned with the visual style feature f_s^I . This alignment is achieved by minimizing the cosine embedding distance between corresponding modality pairs. Through such explicit supervision, the text encoders learn to decompose unstructured clinical language into independent structural and appearance-related control signals. To prevent semantic loss during disentanglement, we introduce a Text Auxiliary Decoder D_T to reconstruct the original text embeddings. The total objective function for this stage is defined as:

$$\mathcal{L}_{text} = \lambda_a\mathcal{D}(f_a^T, f_a^I) + \lambda_s\mathcal{D}(f_s^T, f_s^I) + \mathcal{L}_{rec}^T \quad (2)$$

Hybrid Feature Fusion (HFFM): To leverage the disentangled features f_a^T and f_s^T for fine-grained control over the generation process, we design a Hybrid Feature Fusion Module. We introduce two learnable type embeddings, e_a and e_s , as semantic identities, into the condition embedding $c_{in} = \text{concat}(\mathcal{P}_a(f_a^T) + e_a, \mathcal{P}_s(f_s^T) + e_s)$, to inject into the cross-attention layers of DiT, thereby independently guiding the synthesis of structure and style.

2.3 Generation Process

In the generation stage, we inject the disentangled text features into Diffusion Transformer (DiT) [14] and apply Low-Rank Adaptation (LoRA) [7] for fine-tuning the projection parameters of the attention layers. Furthermore, to ensure color fidelity in the generated images, we introduce an online color distribution loss \mathcal{L}_{cd} , constraining the pixel-level mean and variance of the generated images. The total objective function is $\mathcal{L}_{total} = \mathcal{L}_{mse} + \lambda_{cd}\mathcal{L}_{cd}$.

Table 1. Quantitative comparison on HAM10000, Kvasir-SEG, and BUSI datasets.

Model	HAM10000			Kvasir-SEG			BUSI		
	FID ↓	HFD ↓	KID ↓	FID ↓	KFD ↓	KID ↓	FID ↓	BFD ↓	KID ↓
SD1.5 [17]	100.05	15.45	0.078	119.93	12.34	0.109	159.74	62.15	0.125
SDXL [15]	72.69	8.06	0.058	139.81	9.78	0.154	135.20	55.40	0.098
PixArt- α [3]	68.76	10.14	0.055	67.73	5.24	0.048	100.50	51.94	0.060
MedSegFactory [13]	52.15	4.85	0.042	69.80	4.56	0.058	99.50	43.10	0.055
Med-Art [5]	53.54	9.68	0.049	70.95	5.80	0.051	99.16	43.91	0.062
Ours	51.56	3.22	0.036	71.97	3.70	0.063	98.79	42.60	0.050

3 Experiments and Results

3.1 Dataset and Implementation

Datasets. We validated the effectiveness of our method on three public datasets. The HAM10000 dataset [20] contains 10,015 multi-source dermatoscopic images. The Kvasir-SEG dataset [9] includes 1,000 high-quality polyp images with precise annotations. The BUSI dataset [1] consists of 780 high-quality breast ultrasound images and corresponding masks. We randomly split the datasets into training and testing sets with an 8:2 ratio. To address the scarcity of text descriptions in the original datasets, we generated fine-grained text descriptions rich in anatomical and modal details for each image using the method described in Sec. 2.1. All images were resized to 512×512 resolution to adapt to the generative model.

Implementation Details. Our framework is trained using PyTorch and the Diffusers library on a single A30 GPU. We selected PixArt- α (512×512) as the pre-trained DiT backbone. During the fine-tuning stage, we employed the LoRA strategy (Rank=8) for parameter-efficient training, enabling BF16 mixed precision and Gradient Checkpointing to save GPU memory. The model was trained using the AdamW optimizer with an initial learning rate of 1×10^{-4} , coupled with a Cosine Scheduler with a 500-step warmup. The total training epochs are set to 15. For the color loss, we computed it every $N = 500$ steps with a sampling step of $M = 20$.

3.2 Results

Evaluation of Modality Alignment. To intuitively verify the effectiveness of this mechanism, we present the t-SNE visualization of the feature space before and after modality alignment in Fig. 3. It demonstrates that our model bridges the modality gap, effectively mapping unstructured text descriptions into the disentangled visual latent space.

Comparison with the Image Synthesis Methods. We compared our method with Med-Art [5], SD1.5 [17], SDXL [15], MedSegFactory [13] and PixArt- α [3] on three datasets (Table 1). Generation quality is assessed *w.r.t.* FID, KID, and HFD. On the HAM10000 dataset, our method achieves the best results

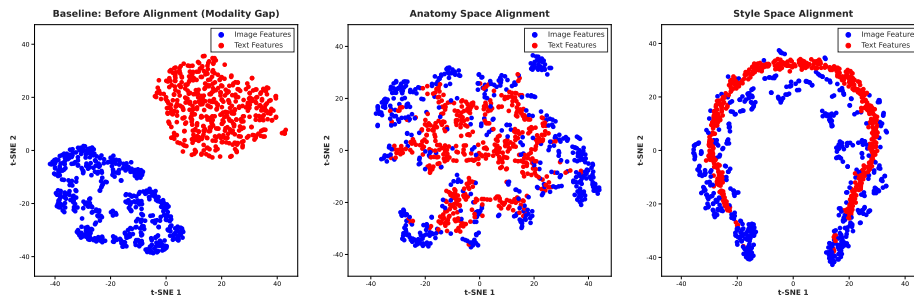


Fig. 3. The t-SNE feature visualization before and after modality alignment. The baseline (Left) exhibits a significant modality gap, where text embeddings are isolated from visual features. In contrast, with our alignment module, the text features are closely aligned with the visual priors in the Anatomy (Middle) and Style (Right) subspaces.

across all metrics. Specifically, FID is reduced to 51.56 and HFD to 3.22, significantly outperforming the strong baseline PixArt- α (FID 68.76). This clearly demonstrates the compelling capability of the visually-guided disentanglement strategy in capturing fine-grained medical features. For the more challenging Kvasir-SEG and BUSI datasets, our method also exhibits competitive performance. Notably, our method consistently maintains the lowest HFD scores (e.g., 3.70 on Kvasir-SEG, better than 5.24 of PixArt- α). This indicates that even when dealing with complex domain gaps, our approach retains a significant advantage in preserving high-frequency details crucial for clinical diagnosis (e.g., mucosal textures and lesion boundaries). Furthermore, as shown in Fig. 4, compared to baseline models like SDXL, images generated by our method are closer to real samples in terms of textural realism and structural consistency. Particularly in dermoscopic images, our model accurately produces complex medical features, such as clearly visible hair details and irregular pigment networks, whereas these subtle features are often over-smoothed or lost in the results of other models. We further compare the model sizes of different methods. Compared with Stable Diffusion 1.5 (1.07B parameters), SDXL (7.5B), PixArt- α (4.9B), and MedSeg-Factory (1.425B), our method requires only 0.833B parameters, achieving a 22% reduction even compared to the smallest baseline.

Downstream Classification Tasks. To verify the clinical utility of the synthetic data, we used the generated images to augment the HAM10000 dataset for training a classifier. Our method achieves the best F1 score (0.6185) and BACC (0.3475) in Table 2, respectively. Although SDXL shows a slight advantage in AUC, our method’s higher F1 and BACC indicate that our generated samples contain richer discriminative features. This confirms that our approach enhances the robustness of diagnostic models and significantly narrows the gap between synthetic and real data.

Ablation Study. We evaluated the effectiveness of key components on the HAM10000 dataset (Table 3). To validate the effectiveness of text guidance, we compared text descriptions (attribute captioning) with only class labels as guid-

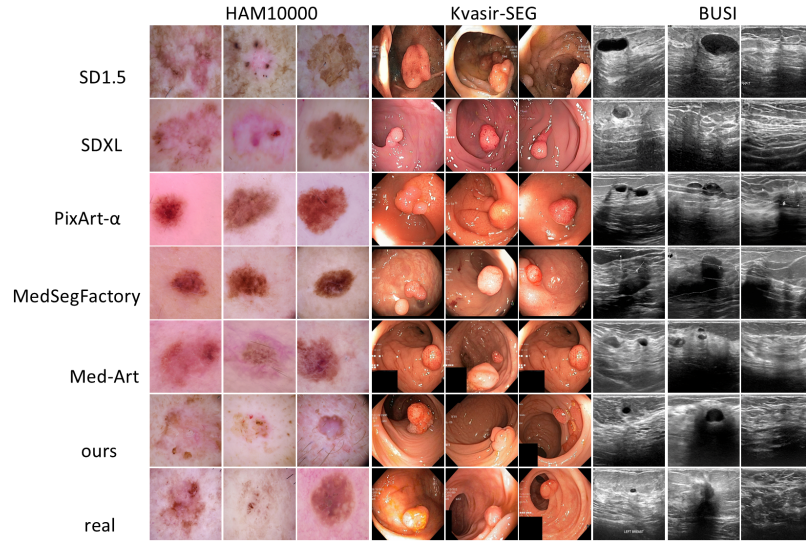


Fig. 4. Visual comparison of image synthesis results.

ance. After removing attribute captioning, FID significantly deteriorated from 51.56 to 69.48. Notably, naive feature concatenation (Naive Feature Concat.) performs even worse than using only class labels (FID 86.24), suggesting that disordered high-dimensional features introduce noise. In contrast, the combination of HFFM and visually-guided disentanglement achieves an FID of 51.56, validating the importance of the structured alignment strategy in generating high-fidelity medical images.

Table 2. Downstream classification performance on HAM10000.

Model	F1 \uparrow	BACC \uparrow	AUC \uparrow
SD1.5	0.595	0.304	0.813
SDXL	0.558	0.339	0.841
PixArt- α	0.536	0.143	0.443
MedSegFactory	0.598	0.345	0.816
Med-Art	0.515	0.333	0.806
Ours	0.619	0.348	0.830
Real Data	0.816	0.657	0.964

Table 3. Ablation study of different components on HAM10000.

Configuration	FID \downarrow	HFD \downarrow	KID \downarrow
w/o Attr. Captioning	69.48	11.34	0.059
Naive Feature Concat.	86.24	8.84	0.073
w/o Disentanglement	53.54	9.68	0.049
Ours	51.56	3.22	0.036

4 Conclusion

In this work, we propose a Visually-Guided Text Disentanglement Diffusion Framework for medical T2I generation. By leveraging cross-modal latent alignment, visual priors are disentangled into anatomical and stylistic representations, which are injected into a DiT backbone via a Hybrid Feature Fusion Module (HFFM) for fine-grained control. Extensive experiments show compelling generation fidelity and diversity, while the generated synthetic data significantly improves downstream diagnostic performance.

References

1. Al-Dhabyani, W., Goma, M., Khaled, H., Fahmy, A.: Dataset of breast ultrasound images. *Data in brief* **28**, 104863 (2020)
2. Alsentzer, E., Murphy, J., Boag, W., Weng, W.H., Jindi, D., Naumann, T., McDermott, M.: Publicly available clinical bert embeddings. In: *Proceedings of the 2nd clinical natural language processing workshop*. pp. 72–78 (2019)
3. Chen, J., Yu, J., Ge, C., Yao, L., Xie, E., Wu, Y., Wang, Z., Kwok, J., Luo, P., Lu, H., et al.: Pixart- α : Fast training of diffusion transformer for photorealistic text-to-image synthesis. *arXiv preprint arXiv:2310.00426* (2023)
4. Chen, W., Wang, P., Ren, H., Sun, L., Li, Q., Yuan, Y., Li, X.: Medical image synthesis via fine-grained image-text alignment and anatomy-pathology prompting. In: *International conference on medical image computing and computer-assisted intervention*. pp. 240–250. Springer (2024)
5. Guo, C., Christensen, A.N., Hannemose, M.R.: Med-art: Diffusion transformer for 2d medical text-to-image generation. In: *MICCAI Workshop on Deep Generative Models*. pp. 57–66. Springer (2025)
6. Guo, P., Zhao, C., Yang, D., Xu, Z., Nath, V., Tang, Y., Simon, B., Belue, M., Harmon, S., Turkbey, B., et al.: Maisi: Medical ai for synthetic imaging. In: *2025 IEEE/CVF Winter Conference on Applications of Computer Vision (WACV)*. pp. 4430–4441. IEEE (2025)
7. Hu, E.J., Shen, Y., Wallis, P., Allen-Zhu, Z., Li, Y., Wang, S., Wang, L., Chen, W., et al.: Lora: Low-rank adaptation of large language models. *ICLR* **1**(2), 3 (2022)
8. Huang, P., Fu, J., Guo, B., Li, Z., Wang, Y., Guo, Y.: Vap-diffusion: Enriching descriptions with mllms for enhanced medical image generation. In: *International Conference on Medical Image Computing and Computer-Assisted Intervention*. pp. 624–633. Springer (2025)
9. Jha, D., Smedsrud, P.H., Riegler, M.A., Halvorsen, P., De Lange, T., Johansen, D., Johansen, H.D.: Kvasir-seg: A segmented polyp dataset. In: *International conference on multimedia modeling*. pp. 451–462. Springer (2019)
10. Jiang, Y., Sun, M., Guo, H., Bai, X., Yan, K., Lu, L., Xu, M.: Anatomical invariance modeling and semantic alignment for self-supervised learning in 3d medical image analysis. In: *Proceedings of the IEEE/CVF International Conference on Computer Vision*. pp. 15859–15869 (2023)
11. Koutsoubis, N., Waqas, A., Yilmaz, Y., Ramachandran, R.P., Schabath, M.B., Rasool, G.: Privacy-preserving federated learning and uncertainty quantification in medical imaging. *Radiology: Artificial Intelligence* p. e240637 (2025)
12. Liu, H., Li, C., Wu, Q., Lee, Y.J.: Visual instruction tuning. In: *Advances in neural information processing systems*. vol. 36 (2024)

13. Mao, J., Wang, Y., Tang, Y., Xu, D., Wang, K., Yang, Y., Zhou, Z., Zhou, Y.: Med-segfactory: Text-guided generation of medical image-mask pairs. arXiv preprint arXiv:2504.06897 (2025)
14. Peebles, W., Xie, S.: Scalable diffusion models with transformers. In: Proceedings of the IEEE/CVF International Conference on Computer Vision. pp. 4195–4205 (2023)
15. Podell, D., English, Z., Lacey, K., Blattmann, A., Dockhorn, T., Müller, J., Penna, J., Rombach, R.: Sdxl: Improving latent diffusion models for high-resolution image synthesis. arXiv preprint arXiv:2307.01952 (2023)
16. Raffel, C., Shazeer, N., Roberts, A., Lee, K., Narang, S., Matena, M., Zhou, Y., Li, W., Liu, P.J.: Exploring the limits of transfer learning with a unified text-to-text transformer. *Journal of machine learning research* **21**(140), 1–67 (2020)
17. Rombach, R., Blattmann, A., Lorenz, D., Esser, P., Ommer, B.: High-resolution image synthesis with latent diffusion models. In: Proceedings of the IEEE/CVF conference on computer vision and pattern recognition. pp. 10684–10695 (2022)
18. Ronneberger, O., Fischer, P., Brox, T.: U-net: Convolutional networks for biomedical image segmentation. In: Medical image computing and computer-assisted intervention—MICCAI 2015: 18th international conference, Munich, Germany, October 5–9, 2015, proceedings, part III 18. pp. 234–241. Springer (2015)
19. Shobayo, O., Saatchi, R.: Developments in deep learning artificial neural network techniques for medical image analysis and interpretation. *Diagnostics* **15**(9), 1072 (2025)
20. Tschandl, P., Rosendahl, C., Kittler, H.: The ham10000 dataset, a large collection of multi-source dermatoscopic images of common pigmented skin lesions. *Scientific data* **5**(1), 1–9 (2018)
21. Yuan, Z., Fang, Z., Huang, Z., Wu, F., Yao, Y.F., Li, Y.: Adapting pre-trained generative model to medical image for data augmentation. In: International Conference on Medical Image Computing and Computer-Assisted Intervention. pp. 79–89. Springer (2024)